Renewable Energy 145 (2020) 466–477

Contents lists available at ScienceDirect

Renewable Energy

journal homepage: www.elsevier.com/locate/renene

Micro cracks distribution and power degradation of polycrystalline solar cells wafer: Observations constructed from the analysis of 4000 samples

Mahmoud Dhimish

University of Huddersfield, Co-Director of Photovoltaics Laboratory, Huddersfield HD1 3DH, United Kingdom

ARTICLE INFO

Article history:
Received 12 December 2018
Received in revised form
1 May 2019
Accepted 11 June 2019
Available online 15 June 2019

Keywords:
Photovoltaic micro cracks
PV defects
Hot-spots
Output power loss
Micro analysis
Electron microscopy imaging

ABSTRACT

In this paper, the impact of Photovoltaic (PV) micro cracks is assessed through the analysis of 4000 polycrystalline silicon solar cells. The inspection of the cracks has been carried out using an electron microscopy, which facilitate the detection of the cracks though the acquisition of both Everhart-Thornley Detector (ETD) and the Back Scatted Electron Diffraction (BSED) image, where it was found that the size micro cracks are ranging from 50 μm to a maximum of 4 mm. Micro cracks have been categorized into two main categories, including cracks in the solar cell front or rear contact. Several remarkable observations have been found, including but not limited to, (i) the output power loss due to micro cracks varies from 0.9% to 42.8%, subject to micro crack type and size, (ii) cracks in solar cells fingers reduce the finger width, resulting an increase in the output power loss by at least 1.7%, and (iii) there is a substantial correlation between PV hot-spots and the presence of micro cracks, while minimum increase in the cell temperature is observed at 7.6 °C.

1. Introduction

Nowadays the lifetime of photovoltaic (PV) modules is an important target for the sustainable development of PV technologies. According to the International Electro-Technical Commission (IEC) 61215 PV qualification standard [1], PV modules are subject to multiple failure modes, ultimately an increase of PV micro cracks [2,3] and PV hot-spotting phenomenon [4,5] have been widely acknowledged. For instance, limited approaches and examination of such faults have been raised, and therefore, further data inspection and validation of typical PV failure have to be assessed and analysed comprehensively.

In order to examine PV micro cracks several methods have been proposed, including but not limited to the Laser scanning technique [6], Electron Microscopy (EM) analysis [7], Photoluminescence (PL) imaging technique [8], and the widely used Electroluminescence (EL) method [9].

F. Haase et al. [10] found that PV micro cracks do not reduce the output power of affected solar cells by more than 2.5%, only if the crack does not harm the fingers or busbars. While, a real-time long-term data analysis of multiple cracked PV modules were analysed by M. Dhimish et al. [11]. It was observed that output power of cracked PV modules ranging from −0.5% to −19.7%; depending on the crack size, orientation and location.

Furthermore, the micro crack analysis on gallium arsenide (GaAs) PV solar cells has been carried out by S. Oh et al. [12]. It was observed that the crack density, defined as the total length of the micro crack per unit area, is found to be in the range from 13.8 to 33.2 cm-1 in all investigated solar cell samples of 1620. On the other hand, the analysis of the output power loss and cracks distribution have not been considered.

PV micro cracks are major cause of hot-spotting. PV hot-spots are a reliability problem in PV modules; this phenomenon is distinguished when a mismatched/cracked solar cell heats up significantly and reduces the PV module output power [13,14]. PV hot-spots can be easily detected using infrared inspection, which nowadays has become a common practice in current PV fault diagnosis as presented in Ref. [15]. However, the correlation between micro cracks and hot-spotting has not widely been considered, while the largest up-to-date study on PV hot-spotting has been reported by our previous work [16]. Furthermore, PV hot-spots can cause a permanent loss in the output power of PV module, and could be reach up to −25% of the PV module maximum power point.

E-mail address: m.a.dhimish@hud.ac.uk.

https://doi.org/10.1016/j.renene.2019.06.057
0960-1481/

PV hot-spotting can be mitigated using various methods such as novel distributive maximum power point tracking (MPPT) method [17,18], adoption of bypass diodes which are parallelized with the PV modules [19], and most recently, a novel two MOSFET layer method developed by Refs. [20,21] improved the output power of hot-spotted PV modules by at least 8% under various environmental conditions.

The main contribution of this work is to present the impact of micro cracks; ranging from 50 μm to a maximum of 4 mm, on the output power performance of solar cells. A total of 4000 cracked samples has been examined. Various major findings have been observed, including:

1) The output power loss due to micro cracks ranging from 0.9 to 42.8%.
2) Cracks in solar cells fingers reduce the finger width, resulting an increase in the power loss.
3) There is a substantial correlation between the hot-spots and micro cracks, multiple results were observed by the reason of the heat expansion due to the micro cracks affect.

2. Methodology

2.1. Electron microscopy

Nowadays in order to examine the micro cracks in the solar wafers, an electron microscopy shown in Fig. 1 has been used. The microscopy is interfaced with a personal computer (PC) using a data acquisition board. The acquisition of both the Everhart-Thornley Detector (ETD) and the Back Scatted Electron Diffraction (BSED) is facilitated using the acquisition board as presented Fig. 1.

The BSED is a microstructural-crystallographic characterization technique normally use to study any crystalline or polycrystalline materials [22], whereas the ETD consists of a secondary electron and back-scatted electron detector, this detector is used to increase the efficiency of existing secondary electron detectors by adding a light pipe to carry the photon signal from the scintillator inside the evacuated specimen chamber of the electron microscopy [23]. In fact, it is not necessary to capture both images, but, for a better resolution and detection of the inspected wafer, both images have been captured.

2.2. Examined solar cell samples

In this article, the examination of 4000 cracked solar cell have been examined; example of multiple samples are shown in Fig. 2(a); showing both front and rear view for diffident types of cracks. All tested samples are dismounted from actual PV modules operated in a field across the UK. The solar cells have been on actual operation for 5–13 years.

All main electrical parameters of the cracked samples have been tested under standard test conditions (STC), where the solar

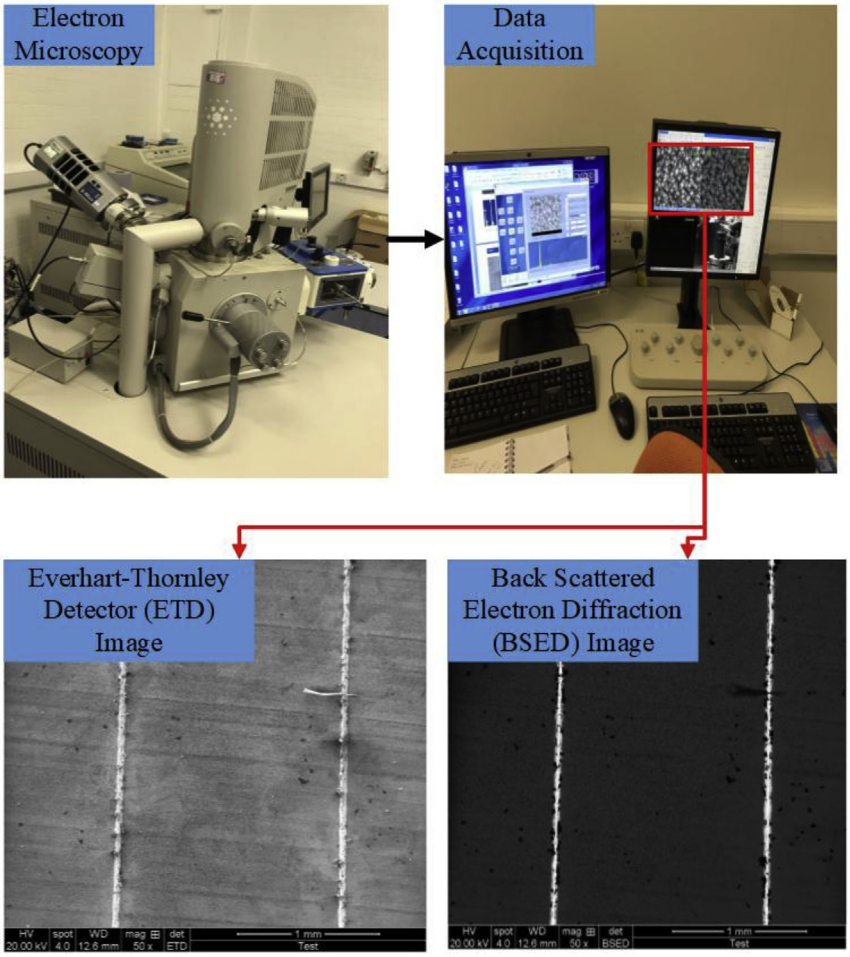

Fig. 1. Electron microscopy facility used to inspect the cracked solar cell samples. The microscope has a data acquisition system which facilitate the monitoring for both the ETD and BSED images using a personal computer.

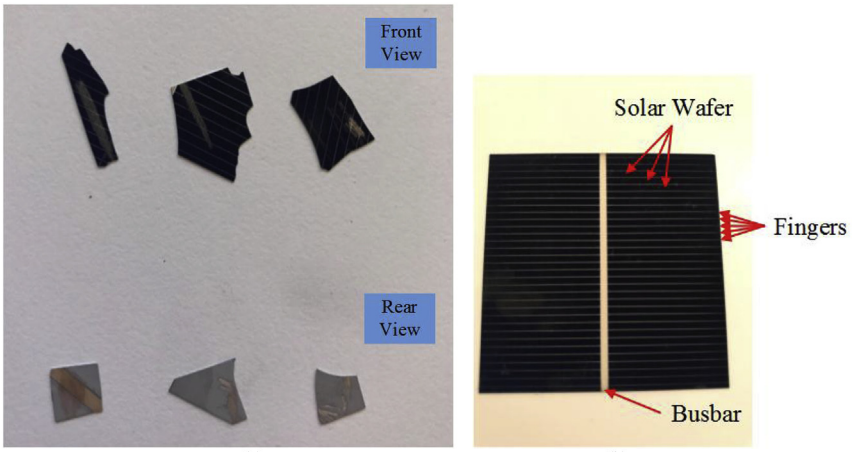

Fig. 2. (a) Example of the front and rear view for multiple examined solar cell wafers, (b) Solar cell wafer, fingers and busbar.

Table 1
Examined solar cells main electrical parameters.

Electrical Parameter	Theoretical Value – Taken form manufacturer data sheet
Voltage at maximum power point (V_{mpp})	0.48 V
Open circuit voltage (V_{oc})	0.61 V
Power at maximum power point (P_{mpp})	3.10 W
Current at maximum power point (I_{mpp})	6.46 A
Short circuit current (I_{sc})	7.12 A

irradiance is equal to 1000 W/m2 and ambient temperature of 25 °C; main electrical parameters are shown in Table 1.

Fig. 2(b) shows the location of the fingers and the solar cell busbar. Solar cell fingers are the metallic rectangular–shape grid connecters which collect the generated current for devilry to the busbar. The busbar is constructed from copper, coated with silver to enhance the current conductivity (front side) as well as to lower oxidization (rear side).

2.3. Distribution and data collection process

The examined solar cells samples have been distributed according to the existence of the micro crack type. The analysis and data collection were distributed across front and rear view/side of the solar cell damage, including:

2.3.1. Front view

1) Wafer + Fingers (Fig. 3(a)): micro cracks affecting both wafer and the fingers of the solar cell.
2) Wafer + Busbar (Fig. 3(b)): existence of micro cracks on solar cell wafer and busbar, but not fingers.
3) Wafer + Fingers + Busbar (Fig. 3(c)): micro cracks affecting the wafer, fingers, and the busbars.

2.3.2. Rear contact

1) Micro cracks affecting rear surface of the solar cell, example shown in Fig. 3(d).
2) Micro cracks affecting both rear surface of the solar cell and the rear busbar, example shown in Fig. 3(e).

All observed micro cracks have a length ranging from 50 μm to a maximum of 4 mm, therefore, the output power analysis as well as the observations in the rest of the article are based on this assumption, and ultimately, different crack length would result different observations.

The percentage of occurrence of the micro cracks in all tested samples are summarized as follows:

1) Wafer + Fingers presenting 39%; 1560 samples.
2) Wafer + Busbar presenting 17%; 680 samples.
3) Wafer + Fingers + Busbar presenting 36%; 1440 samples.
4) Rear surface presenting 6%; 240 samples.
5) Rear surface + Rear Busbar presenting 2%; 80 samples.

It is worth noting that the number of cracked busbars or fingers has not been considered in the data analysis. There are two reasons behind this choice including, **(i)** the data collection and analysis of the output power loss will fluctuate rapidly if the number of fingers and busbars are counted, and **(ii)** in order to draw relevant conclusions with the consideration of multiple case studies, it would help to classify which micro crack type/category has the most significant impact on the output power loss; resulting a generic/extensive gained knowledge on the studied samples, where the outcomes can be used extensively across a number of other studies, including PV degradation, PV manufacturing analysis and solar cell micro cracks detection systems.

3. Results

3.1. Power loss analysis

In this section, the evaluation of the power loss of all examined PV solar cell is presented. The measured power loss of the solar cells is captured while experimentally illuminating the cells under standard test conditions (STC), where the solar irradiance is equal

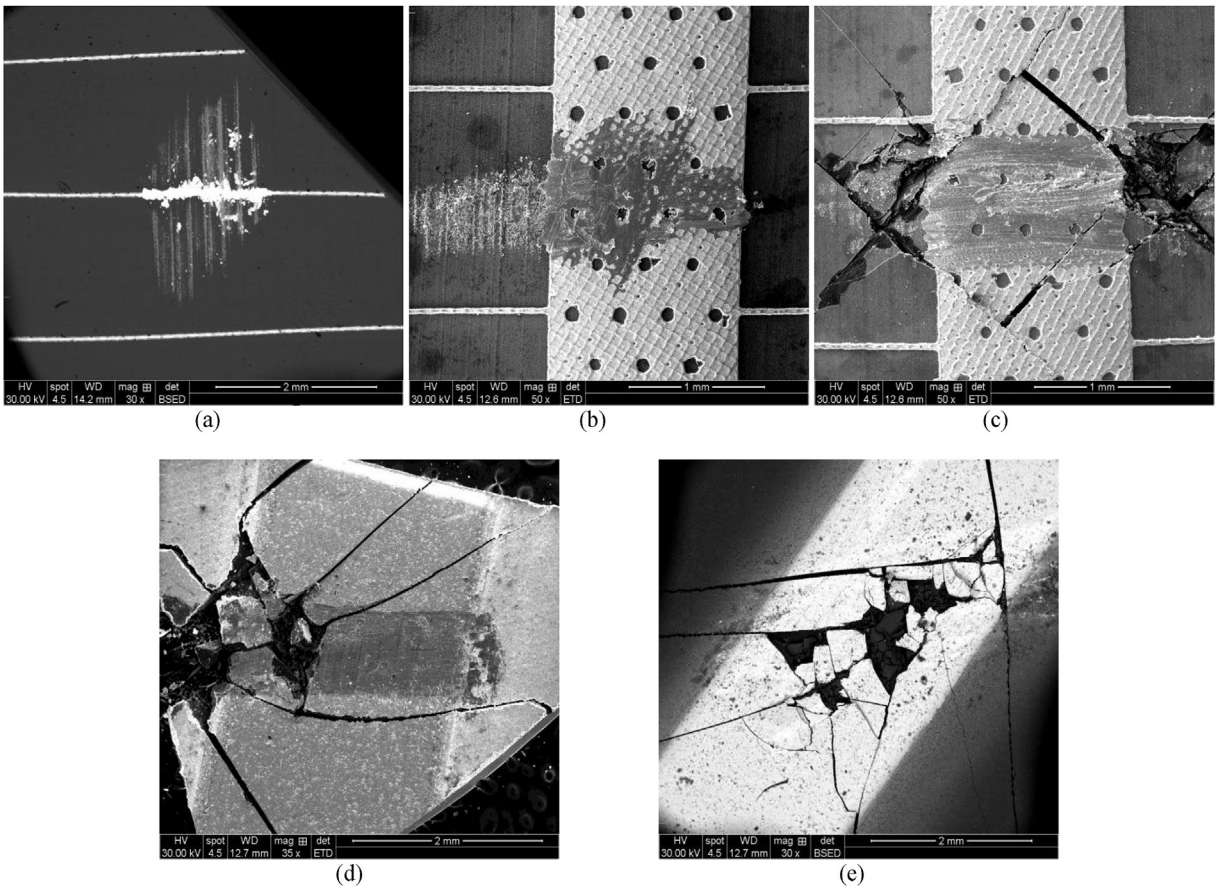

Fig. 3. Examples of the distribution for the micro cracks in different solar cell samples. (a) Micro cracks affecting solar cell wafer and fingers, (b) Micro cracks affecting solar cell wafer and busbars, (c) Micro cracks affecting solar cell wafer, fingers and busbar, (d) Micro cracks in the rear surface of the solar cell, (e) Micro cracks affecting rear surface of the solar cell as well as the rear busbar.

to 1000 W/m^2, and cell surface temperature of 25 °C, the experimental setup is shown in Fig. 6(b). The output power loss is measured by the following formula:

$$Power\ Loss(\%) = 100 - \left(\frac{P_{Micro\ cracked\ solar\ cell}}{P_{Theoretical\ maximum\ power}} \times 100 \right) \quad (1)$$

where $P_{Micro\ cracked\ solar\ cell}$ is the actual measured output power of the tested micro cracked solar cell sample, whereas $P_{Theoretical\ maximum\ power}$ is the theoretical power taken from the datasheet; the value for the theoretical power is equal to 3.1 W, presented earlier in Table 1.

According to Fig. 4(a), the solar cell samples affected by cracks in the front contact have a power loss ranging from:

1) Cracks in Wafer + Finger: -1.7% to −13.5%.
2) Cracks in Wafer + Busbar: -0.9% to −17.1%.
3) Cracks in Wafer + Finger + Busbar: -8.9% to −42.8%.

Evidently, the cracks affecting solar wafer, fingers and the busbar have the uppermost power loss, with mean of 25.52%, whereas the second maximum mean output power loss of 9.01% is obtained for the solar cells affected by micro cracks in the solar wafer and the busbar. The minimum output power loss is observed for solar cells that are affected by micro cracks across the wafer and fingers, their mean output power loss is equal to 7.59%.

According to the solar cell samples affected by rear contact micro cracks, it was observed that loss in the output power is very limited (mean of 1.48%) for the rear surface cracks, however, there are an increase in the output power loss due to the rear contact cracks affecting both surface and the rear busbar, where it was found that the mean output power loss is equal to 7.99%.

It is noticeable that front contact micro cracks have the most significant impact on the overall performance of the solar cells because these cracks affects the surface of the junction, ultimately limiting the amount of solar energy to be extracted by the cell. On the other hand, the output power loss for micro cracked rear surface is far less than the front contact, since it is much further away from the junction, whereas the rear busbar plays significant role in driving the solar cell current, therefore, cracks in rear and front busbar have a much higher output power loss.

There are a number of observations that have been identified using the studied sample set, including the correlation between micro cracks and hot-spots in the micro cracked solar cells. These observations are discussed in the following sections.

3.2. Effect of breakdown/micro-cracks in solar cells fingers

Due to the existence of micro cracks, it was observed that out of all examined samples, almost there are 1500 samples that has a breakdown/cracks in the solar cell fingers, resulting a less forward current generation of the solar cell. Two examples of the micro crack, damage and discontinuity in the solar cell fingers are shown in Fig. 5(a) and (b).

There is an increase in the output power loss due to the cracked/

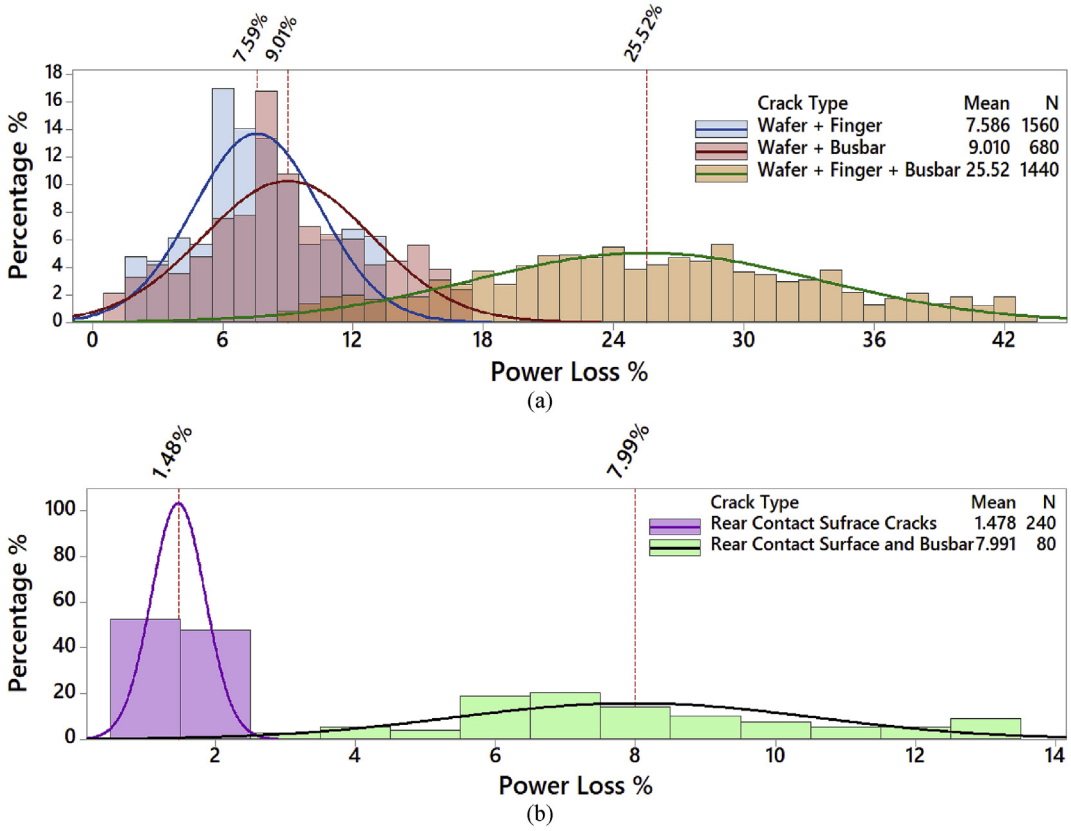

Fig. 4. Power loss analysis of the cracked solar cell samples. (a) Front contact crack-types, (b) Rear contact crack-types.

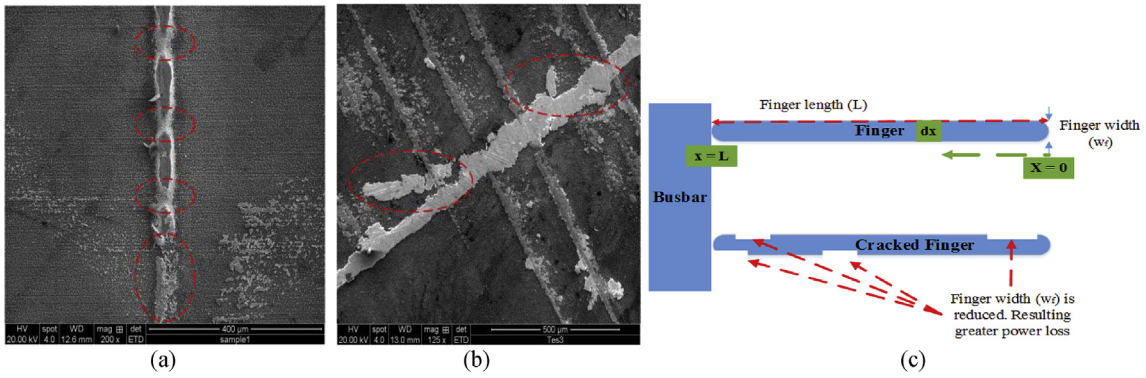

Fig. 5. (a) Cracked – non discontinuity in solar cell finger, sample 1, (b) Cracked – non discontinuity in solar cell finger, sample 2, (c) Illustration on the fingers main parameters, where the width of the cracked finger is reduced resulting a greater power loss.

damaged fingers. In order to calculate the power loss in a single finger, the integration of the length for the finger starting from 0 to L (shown in Fig. 5(c)) gives the power loss as calculated by (2).

$$Power\ loss = \int_{x=0}^{x=L} \frac{\left(xJ_{MPP}S_f\right)^2}{w_f\ d_f} d_x = \frac{1}{3}L^3 J_{MPP}^2 S_f^2 \frac{\rho_f}{w_f\ d_f} \tag{2}$$

where $L = 2cm$ is the finger length, $J_{MPP} = 30\ mA/cm^2$ is the current at maximum power point, $S_f = 2mm$ is the finger spacing, $\rho_f = 1.82 \times 10^{-8}\ \Omega m$ is the effective resistivity of the metal, $w_f = 25\ \mu m$ is the finger width, and $d_f = 13\ \mu m$ corresponds to the finger depth (or height); all parameters values are taken from solar cell manufacturer datasheet.

As shown in Fig. 7(a) and (b), the measured total power loss for the solar cell finger without the existence of micro cracks is equal to 3.8%, while it is increased to 5.0% for the cracked finger sample. The main reason in the increase of the power loss is due to the decrease in the finger width. Therefore, According to (2), if the width of the finger w_f decrease, the finger power loss will increase. Furthermore, the cracks in the solar cell fingers increase the heat-level of the affected solar cell, because the forward current will be delivered though marginal size of metal (due to the reduction of the finger width size). Consequently, this will create a hot-spot in the finger and will reduce the forward current delivered by the cracked cell. Fig. 6(a) shows a cracked solar cell sample tested under STC conditions, where two fingers are cracked.

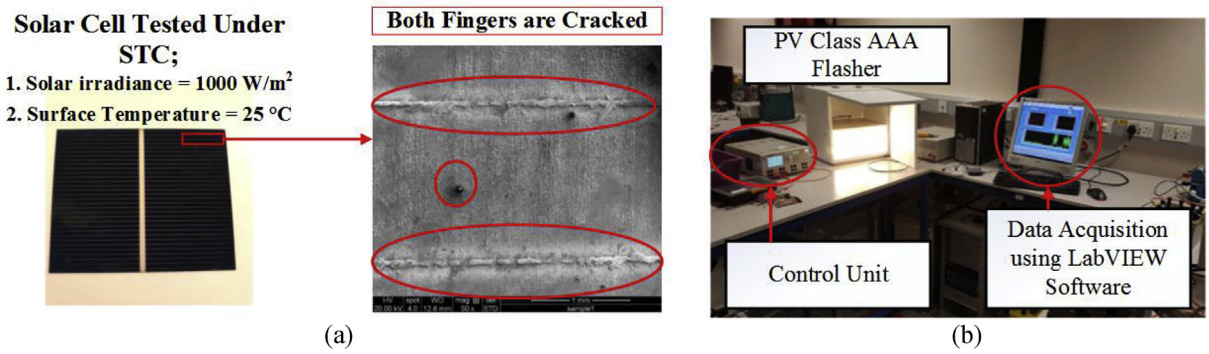

Fig. 6. (a) Cracked solar cell tested under STC, (b) PV Class AAA Flasher setup.

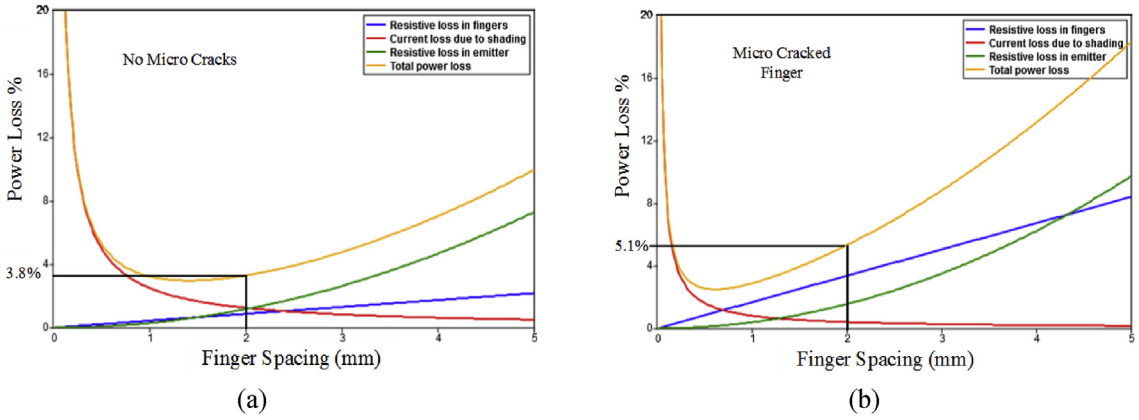

Fig. 7. (a) Power loss estimation (~3.8%) for finger without existence of micro cracks, (b) Power loss estimation (~42%) for finger including micro cracks.

The obtained results shown in Fig. 7 are measured using the analysis of a healthy vs. micro cracked solar cell sample under STC. The setup of the class AAA LED flasher is shown in Fig. 6(b). The solar cell sample has been placed inside the LED-based flasher, whereas a control unit is used to attain a light intensity of 1000 W/m2 and ambient temperatures of 25 °C. Thereafter, the output power, current and resistive loss are measured using a data acquisition system which uses LabVIEW software. It is also worth noting that all tested samples get an illumination of 1000 W/m2 for a period of 5 ms, this is the fastest rate of change that is possible for the flasher to switch its mode from the on/off state. Therefore the observed heat-map and thermal-image corresponds to the actual change of the heat across the surface of the solar cell.

The output heat-map/thermal-image of the solar cell is shown in Fig. 8. By contrast with the results shown in Fig. 8(a), after ten seconds of evaluating the solar cell sample under STC, the temperature of the cracked area raised to 72.6 °C, whereas adjacent regions started to heat-up to a limit of 42.5 °C. Interestingly, due to the expansion of the heat over the whole solar cell, the heat of the cracked area started to decrease due to the flow of the heat over the full cell sample. In Fig. 8(b), thermal image of the solar cell sample is captured after 60 s, it is evident that the cracked area has a lower temperature of 43.9 °C, but more area of the solar cell is affected by a rise in the temperature. In addition, according to Fig. 8(c), after 120 s (the test sample was still under STC), the solar cell sample almost have an identical temperature level of 34.3 °C, compared to original temperature of 26.7 °C, therefore, the increase of the solar cell temperature due to the existence of the micro cracks is raised by 7.6 °C. It is worth noting that this temperature level remains same after 120 s. This result confirms that micro cracks in solar cells cause hot-spots, where the main heat source of the cell is spread from the original cracked area, and it heats up significantly due to the excitation of the electrons through a thinner width of the metal carrying the current either in the fingers or busbars, subsequently an increase in the solar cell temperature will be granted, as well as an increase in the output power loss would highly be expected.

By contrast with above results, the heat is transferred from the hot-spot area to the rest of the solar cell due to the concept of heat by conduction. Conduction is the transfer of heat energy through a solid by the collision and vibration of molecules in the solar cell, without movement of the bulk material. For example, the hot-spotted area molecules interact with neighboring molecules, transferring some of their energy (heat) to these adjacent particles. And since this heat would decrease in the hot-spotted area and increase in the adjacent area, the solar cell temperature went steady. This phenomenon is well-known by the transient conduction where the heat is not only transferred through the solid using the vibration of the molecules but also as a function of time [24].

According to Ref. [25] it was observed that 78% of the reverse power is turned into heat at the hot-spot area. The remaining fraction of the power was evenly distributed over the cell, accounting for the normal reverse current, possible contact resistance and additional small shunts. Consequently, the distribution of the heat over the cell is generated due to the reverse current flowing from the hot-spotted area throughout the cell using the adjacent fingers and busbar, successively reducing the output generated power of the affected solar cell. Similarly, authors in Ref. [26] presented a new method which provides simple and fast evaluation of the hot-spotted solar cells. It was shown that the heat of the affected solar cell by possible hot-spots could be distributed across

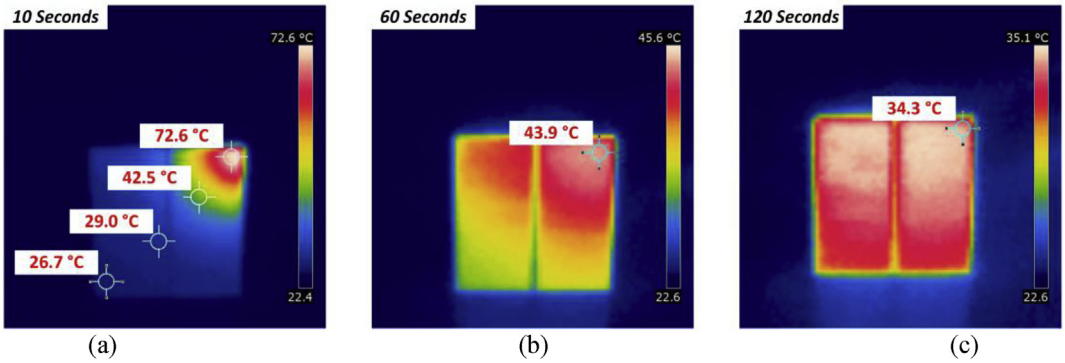

Fig. 8. Heat-Map distribution of the cracked solar cell shown in Fig. 6, operating under STC, images are captured using FLIR thermal camera. (a) After 10 s, (b) After 60 s, (c) After 120 s – this level of temperature remains steady.

the adjacent locations after a period of 60 ms, where the main cause of the heat distribution is due to the existence of non-cracked fingers and busbars.

In order to determine the I-V and P-V curves of the solar cell sample under STC, an experiment has been carried out using the class AAA LED flasher shown in Fig. 6(b). The obtained I-V and P-V curves are presented in Fig. 9. Compared to the theoretical predictions (discussed earlier in Table 1), the solar cell sample has almost equal V_{mpp} of 0.48 V. However, there is drop in the I_{mpp} by 0.286 A; I_{mpp} (theoretical: 6.46 A) – I_{mpp} (cracked solar cell: 6.174 A). Resulting an output power loss of 4.39%; calculated as follows:

$$Power\ Loss(\%) = 100 - \left(\frac{2.964\ (P_{Micro\ cracked\ solar\ cell})}{3.1\ \left(P_{Theoretical\ maximum\ power}\right)} \times 100 \right)$$

$$= 4.39\%$$

Another example of cracked fingers has been examined, the cracked cell is shown in Fig. 10. The cell is affected by three cracked fingers, where it is evident that there is a discontinuity in the finger connections, this would result an increase in the amount of heat generated by this particular case.

The examination of the heat-level of the solar cell, starting at 0 s; where the cell has not yet been tested under STC, ending up with 100 s, where at this stage the cell temperature remains at constant level. The results of the experiment are shown in Fig. 11.

At zero seconds, the temperature of the cell is equal to 24.3 °C. The temperature of the cracked area raised to 105.1 °C after 20 s of testing the cell under STC. Ultimately, the heat-level of the cracked would decrease, due to the expansion of the heat over the cell, resulting a temperature levels of:

1) 83.6 °C (40 s)
2) 70.9 °C (60 s)
3) 55.8 °C (80 s)
4) 40.2 °C (100 s) - this level of temperature remains consistent

In contrast with the results of the heat-distribution, the solar cell had an increase in the temperature of about 15.9 °C; final temperature level 40.2 °C – original temperature level 24.3 °C. Therefore, this results confirms that micro cracks in solar cells are one of the main cause of PV hot-spotting, as well as, the increase in the size of cracked area, ultimately will increase the heat-level of the hot-spot in the affected solar cell.

The solar cell sample has been tested under STC. The obtained I-V and P-V curves are presented in Fig. 12. Compared to the theoretical predictions (discussed earlier in Table 1), the sample has almost equal V_{mpp} of 0.47 V. However, there is drop in the I_{mpp} by 0.662 A. Hence, the output power loss is equal to 12.09%; calculated as follows:

$$Power\ Loss\ (\%) = 100 - \left(\frac{2.725\ (P_{Micro\ cracked\ solar\ cell})}{3.1\ \left(P_{Theoretical\ maximum\ power}\right)} \times 100 \right)$$

$$= 12.09\%$$

3.3. Impact of busbars and rear contact surface damage due to micro cracks and poor manufacturing/soldering practice

Due to the Another remarkable result was observed while examining the solar cell samples, out of 4000 there are 680 affected by cracks in the busbar. The micro cracks in the busbar leads to

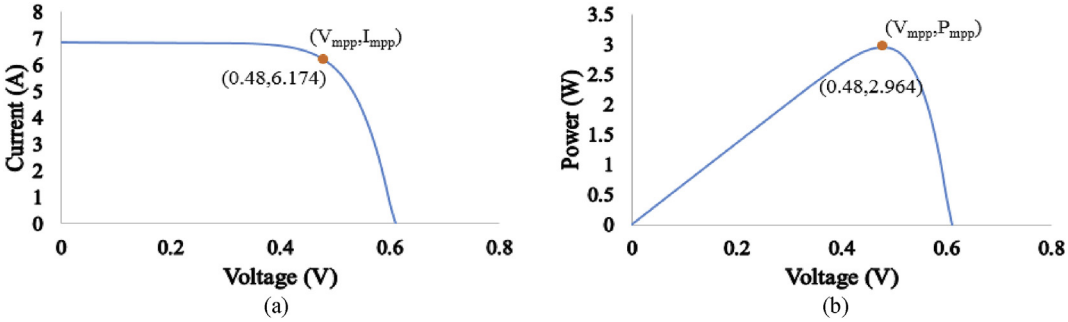

Fig. 9. Obtained I-V & P-V curves of the cracked solar cell sample shown in Fig. 6(a) under STC.

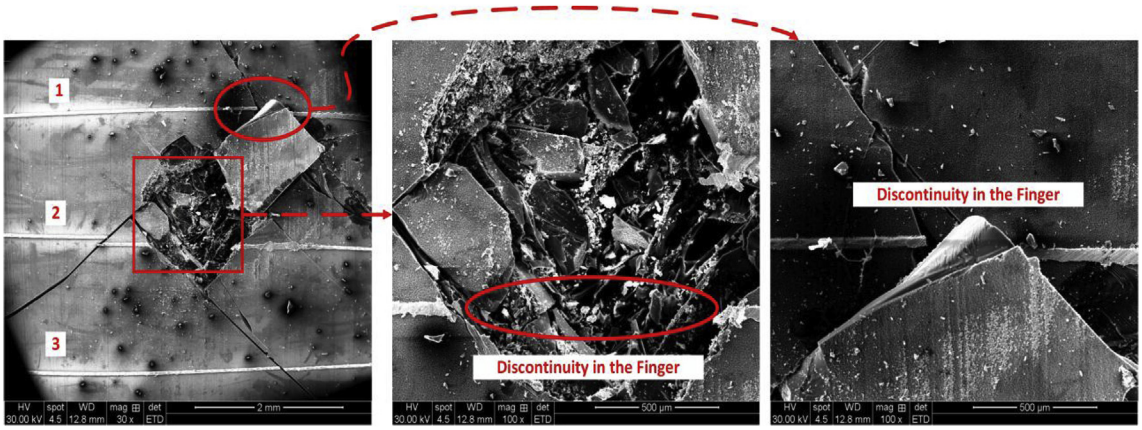

Fig. 10. Micro crack affecting three fingers – there is a discontinuity in the finger connection to the main busbar.

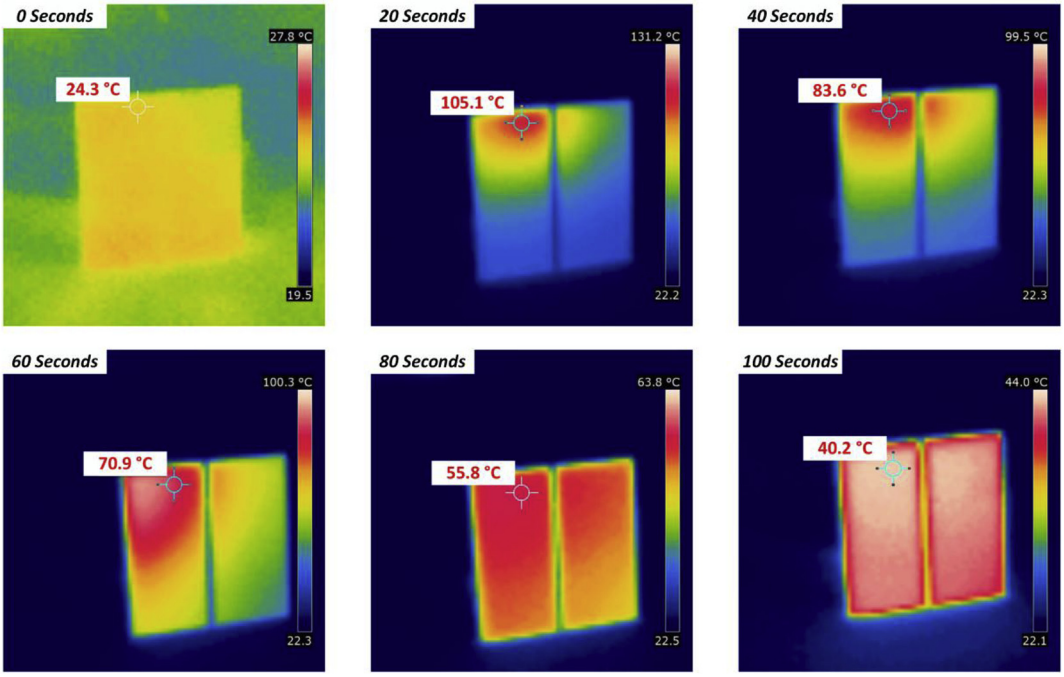

Fig. 11. Heat-Map distribution from 0 to 100 s of the cracked solar cell shown in Fig. 9; the solar cell is operated under STC.

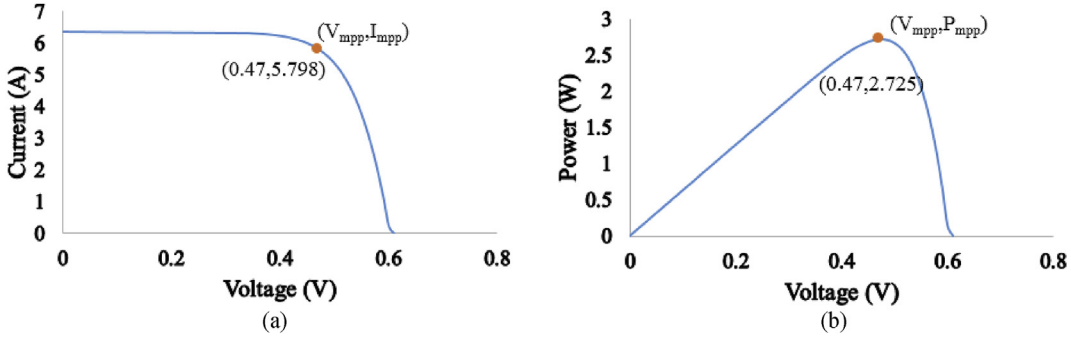

Fig. 12. Obtained I-V & P-V curves of the cracked solar cell sample shown in Fig. 10 under STC.

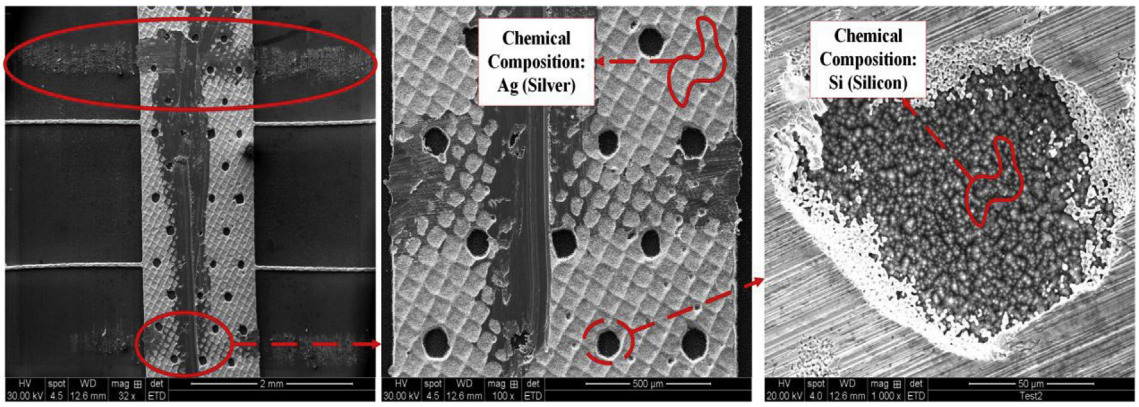

Fig. 13. Micro cracks and soldering mismatch in a solar cell busbar.

significant damage in the metal driving the current from the fingers outer to an external circuit. On the other hand, almost 380 solar cell samples are affected by poor soldiering.

A sample showing a poor adjustment of the busbar metal is shown in Fig. 13. As noticed, there are a number of cracks in the solar wafer, while the busbar contains multiple cracks. The silicon (Si) chemical composition is present instead of original chemical composition of the silver (Ag). This poor busbar structure leads to a second breakdown in the solar cell sample, ultimately causing hot-spot.

The solar cell shown in Fig. 13 has been examined under STC (experimental setup similar to Fig. 6). The solar cell has a micro crack as well as poor soldiering in the busbar. It is expected after 10 s the heat would increase significantly in the cracked area, and as shown in Fig. 14(a), the temperature of the cracked area increased to abnormal level of 91.4 °C. After 60 s, the heat started to expand over the entire solar cell, where the busbar and the cracked area has a temperature of 77.3 °C, as presented in Fig. 14 (b).

According to Fig. 14(c), the heat is spread all over the solar cell sample, the temperature is equal to 38.2 °C; this temperature level stays consistent after 120 s. Therefore, this experiment proves that cracks in solar cell busbars have a significant impact on the solar cell heat level, ultimately initiating hot-spots.

I-V and P-V curves for the solar cell sample have been measured under STC, results are presented in Fig. 15. The measured V_{mpp} of 0.48 V is identical with the theoretical predictions (presented earlier in Table 1). However, there is a drop in the maximum output current of 0.15 A; I_{mpp} (theoretical: 6.46 A) – I_{mpp} (cracked solar

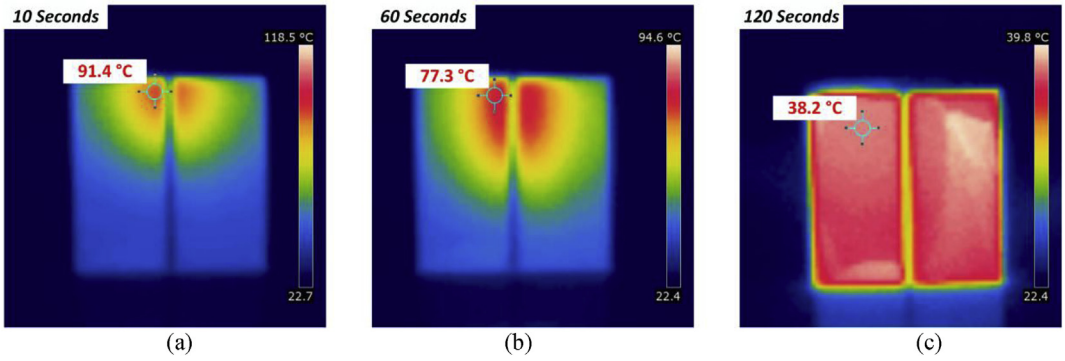

Fig. 14. Heat-Map distribution of the cracked solar cell shown in Fig. 8. (a) After 10 s of operating the solar cell under STC, (b) After 60 s, (c) After 120 s – this level of temperature remains consistent.

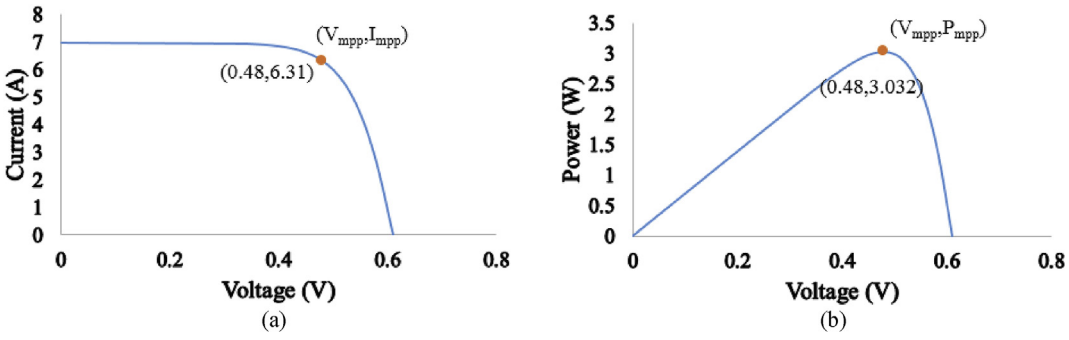

Fig. 15. Obtained I-V & P-V curves of the cracked solar cell sample shown in Fig. 13 under STC.

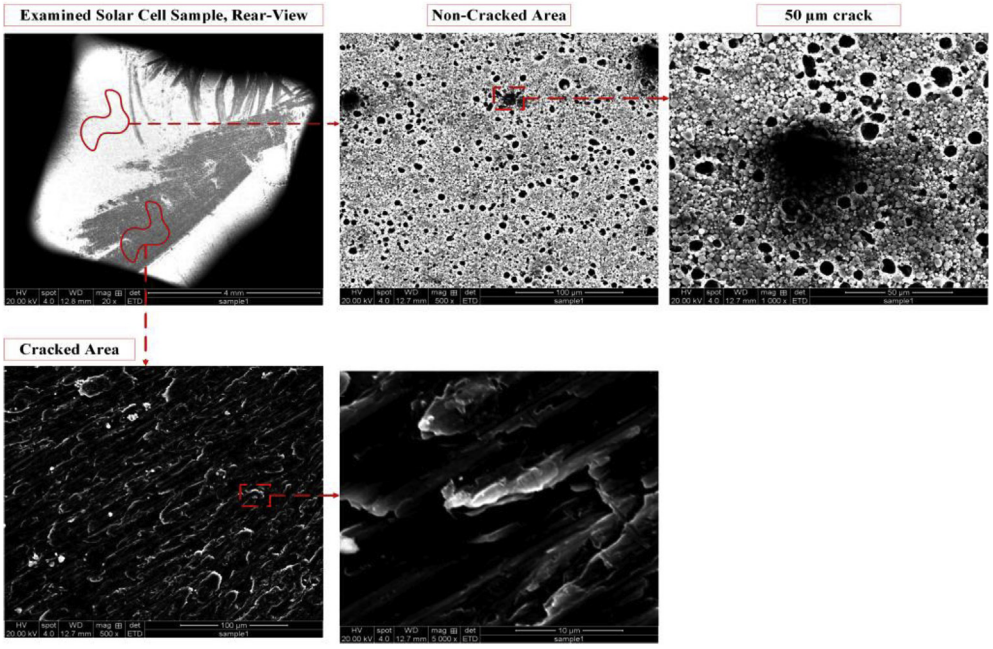

Fig. 16. Micro cracks affecting rear contact of a solar cell.

cell: 6.31 A). Resulting a loss in the output power equals to 2.19%; calculated as follows:

$$Power\ Loss\ (\%) = 100 - \left(\frac{3.032\ (P_{Micro\ cracked\ solar\ cell})}{3.1\ \left(P_{Theoretical\ maximum\ power}\right)} \times 100 \right) = 2.19\%$$

The rear contact of a typical solar cell is far less important than the front contact, since it is much further away from the junction. However, the design of the rear contact is becoming progressively essential as overall efficiently increases and the solar cells become thinner. During the investigation of the rear contact of the examined solar cells, it was found that 320 solar cells are cracked; 240 samples are cracked in the surface, while 80 samples are cracked in both the surface and the rear busbar. Fig. 16 shows the rear contact/view of an examined solar cell sample. The difference between the cracked and non-cracked area are shown in the figure. Principle, the cracked area consists of two chemical composition of aluminum (Al) and silicon (Si), while the non-cracked area is only made of aluminum.

As shown in Fig. 16, the non-cracked area has multiple micro cracks of 50 μm width; nevertheless, it does not have a noteworthy loss to the solar cell rear contact. However, the actual size of cracked rear area varies from 4 mm to 300 μm. This damage in the rear contact of solar cell resulting a limited open circuit voltage (V_{oc}), subsequently will reduce the efficiency of the cell. In light of what was observed during the experiments, hot-spotting phenomena has no correlation with the presence of micro cracks in solar cells rear contact surface.

Likewise, Fig. 17(a) shows a rear contact image for a solar cell samples affected by micro cracks in the surface and busbar. The solar cell was tested under STC, while the temperature of the cell has been captured and reported in Fig. 17(b); image is taken from 0 s to 100 s.

At zero seconds, the temperature of the cell is equal to 25.2 °C. The temperature of the cracked area raised to 78.2 °C after 20 s. Eventually, the heat-level of the cracked area will decrease, due to the expansion of the heat over the cell and would result a temperature levels of 67.7 °C (40 s); 61.9 °C (60 s); 51.6 °C (80 s); and 42.3 °C (100 s), this level of temperature remains consistent. In light with the results of the heat-distribution, the solar cell had an increase in its temperature of 17.1 °C; final temperature level 42.3 °C − original temperature level 25.2 °C. Therefore, this result shows the impact of micro cracks on the rear contract temperature, while it was evident that there is an abnormal increase in the cell temperature while performing at STC.

I-V and P-V curves for the solar cell sample have been measured under STC, results are presented in Fig. 18. The measured V_{mpp} of 0.48 V is identical with the theoretical predictions (presented earlier in Table 1). However, there is a drop in the maximum output current of 0.215 A; I_{mpp} (theoretical: 6.46 A) − I_{mpp} (cracked solar cell: 6.245 A). Resulting a loss in the output power equals to 3.29%; calculated as follows:

$$Power\ Loss\ (\%) = 100 - \left(\frac{2.998\ (P_{Micro\ cracked\ solar\ cell})}{3.1\ \left(P_{Theoretical\ maximum\ power}\right)} \times 100 \right) = 3.29\%$$

4. Conclusion

The impact of Photovoltaic (PV) micro cracks has been assessed through the analysis of 4000 polycrystalline silicon solar cells. The inspection of the cracks has been carried out using an electron microscopy, which facilitate the detection of the cracks though the acquisition of both Everhart-Thornley Detector (ETD) and the Back Scatted Electron Diffraction (BSED) image, where it was found that the size micro cracks are ranging from 50 μm to a maximum of 4 mm. Micro cracks have been categorized into two main categories, including:

1) Front contact cracks affecting wafer, fingers and busbar.
2) Rear contact cracks affecting rear furnace and the busbar.

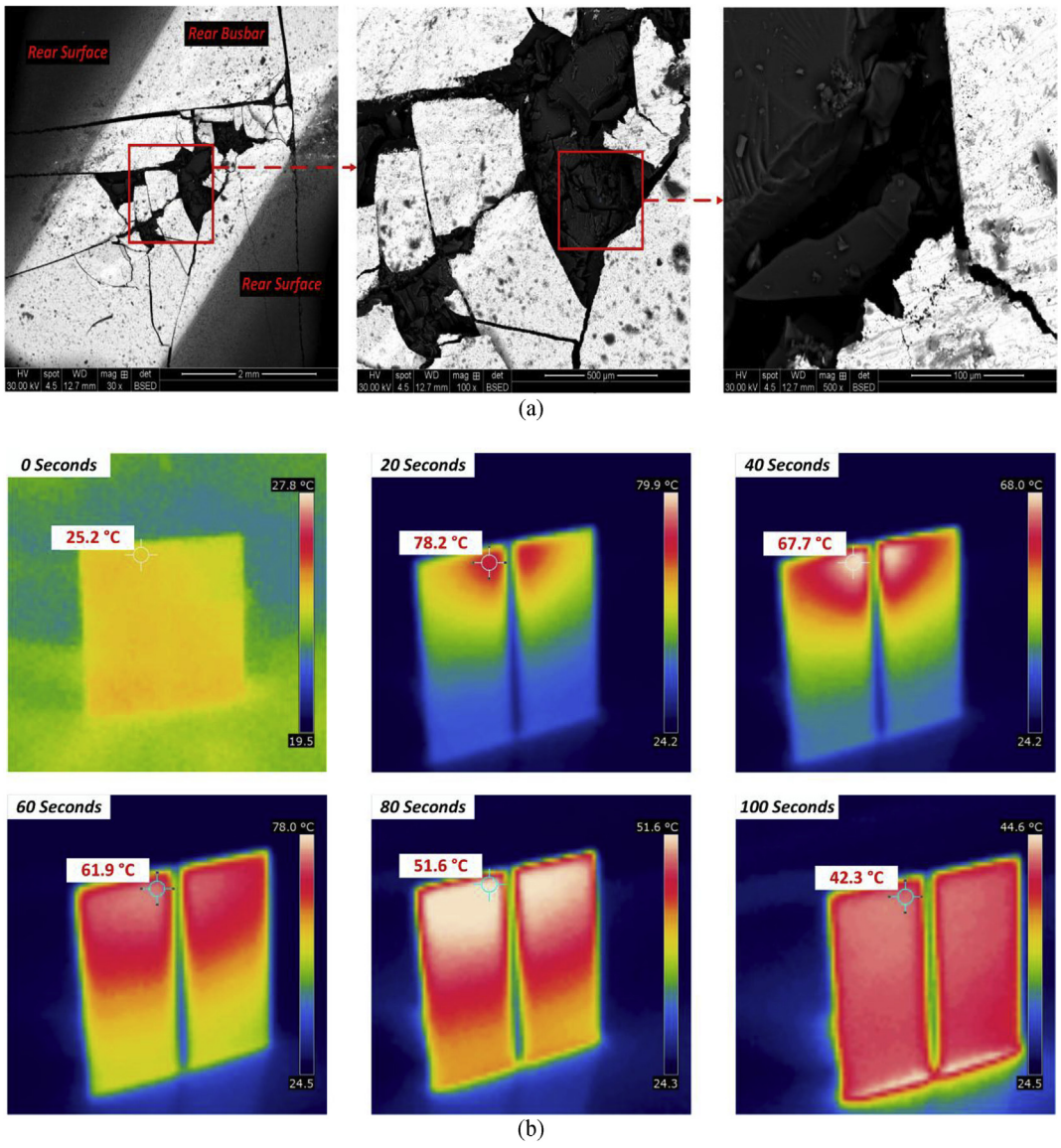

Fig. 17. Micro cracks affecting rear contact surface and busbar of a solar cell. (a) Crack affected rear surface and busbar; images magnification of 2 mm, 500 μm and 100 μm, (b) Heat-Map distribution from 0 to 100 while the solar cell is illuminated under STC.

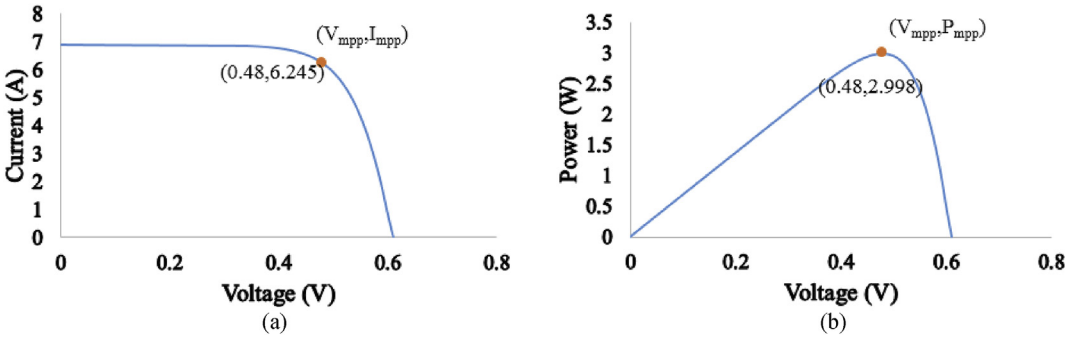

Fig. 18. Obtained I-V & P-V curves of the cracked solar cell sample shown in Fig. 17(a) under STC.

Various remarkable observations have been found, including:

1) The output power loss due to micro cracks ranging from 0.9 to 42.8%.
2) Cracks in solar cells fingers reduce the finger width, resulting an increase in the power loss by at least 1.7%.
3) There is a significant correlation between PV hot-spots and existence of micro cracks. While the temperature of a cracked solar cell sample could increase by 7.6 °C or more, resulting a permanent hot-spots in the affected cell.

In future, it is intended to investigate the mitigation of micro cracks in solar cells, and develop a novel intelligent detection system to locate and possibly evaluate the impact of such cracks on the output power performance of solar cells.

Author agreement/Declaration

The author has approved the final version of the manuscript being submitted. He warrant that the article is the author's original work, hasn't received prior publication and isn't under consideration for publication elsewhere. Mahmoud confirms he is sole author for all presented results in the article.

Conflicts of interest

The author declare that there is no conflict of interest for the submitted manuscript, (Conflict of interest: None).

Funding

The author declare that no funding belongs to the submitted manuscript (Funding source: None).

References

[1] IEC 61215, International Standard, Crystalline Silicon Terrestrial Photovoltaic (PV) Modules – Design Qualification and Type Approval, European Committee for Electrotechnical Standardizations. Photovoltaic (PV) Module Safety Qualification, 2006.
[2] C. Borri, M. Gagliardi, M. Paggi, Fatigue crack growth in Silicon solar cells and hysteretic behaviour of busbars, Sol. Energy Mater. Sol. Cell. 181 (2018) 21–29.
[3] M. Dhimish, V. Holmes, P. Mather, C. Aissa, M. Sibley, Development of 3D graph-based model to examine photovoltaic micro cracks, J. Sci. Adv. Mater. Devices 3 (3) (2018) 380–388.
[4] A. Aly, S.S. Jensen, A.B. Pedersen, Solar power potential of Tanzania: identifying CSP and PV hot spots through a GIS multicriteria decision making analysis, Renew. Energy 113 (2017) 159–175.
[5] M. Dhimish, V. Holmes, B. Mehrdadi, M. Dales, P. Mather, Output-power enhancement for hot spotted polycrystalline photovoltaic solar cells, IEEE Trans. Device Mater. Reliab. 18 (1) (2018) 37–45.
[6] N. Srećković, N. Lukač, B. Žalik, G. Štumberger, Determining roof surfaces suitable for the installation of PV (photovoltaic) systems, based on LiDAR (Light Detection and Ranging) data, pyranometer measurements, and distribution network configuration, Energy 96 (2016) 404–414.
[7] C. Xiang, X. Zhao, L. Tan, J. Ye, S. Wu, S. Zhang, L. Sun, A solar tube: efficiently converting sunlight into electricity and heat, Nano Energy 55 (2019) 269–276.
[8] S.M. El-Bashir, F.F. Al-Harbi, H. Elburaih, F. Al-Faifi, I.S. Yahia, Red photoluminescent PMMA nanohybrid films for modifying the spectral distribution of solar radiation inside greenhouses, Renew. Energy 85 (2016) 928–938.
[9] K.G. Bedrich, W. Luo, M. Pravettoni, D. Chen, Y. Chen, Z.,. Wang, Y. Wang, Quantitative electroluminescence imaging analysis for performance estimation of PID-influenced PV modules, IEEE J. Photovolt. 8 (5) (2018) 1281–1288.
[10] F. Haase, J. Käsewieter, S.R. Nabavi, E. Jansen, R. Rolfes, M. Köntges, Fracture probability, crack patterns, and crack widths of multicrystalline silicon solar cells in PV modules during mechanical loading, IEEE J. Photovolt. 8 (6) (2018) 1510–1524.
[11] M. Dhimish, V. Holmes, M. Dales, B. Mehrdadi, Effect of micro cracks on photovoltaic output power: case study based on real time long term data measurements, Micro & Nano Lett. 12 (10) (2017) 803–807.
[12] S. Oh, D.H. Jun, K.W. Shin, I. Choi, S.H. Jung, J.,. Choi, E. Yoon, Control of crack formation for the fabrication of crack-free and self-isolated high-efficiency gallium arsenide photovoltaic cells on silicon substrate, IEEE J. Photovolt. 6 (4) (2016) 1031–1035.
[13] M. Bressan, A. Gutierrez, L.G. Gutierrez, C. Alonso, Development of a real-time hot-spot prevention using an emulator of partially shaded PV systems, Renew. Energy 127 (2018) 334–343.
[14] M. Dhimish, V. Holmes, P. Mather, M. Sibley, Novel hot spot mitigation technique to enhance photovoltaic solar panels output power performance, Sol. Energy Mater. Sol. Cell. 179 (2018) 72–79.
[15] D. Rossi, M. Omaña, D. Giaffreda, C. Metra, Modeling and detection of hotspot in shaded photovoltaic cells, IEEE Trans. Very Large Scale Integr. (VLSI) Syst. 23 (6) (2015) 1031–1039.
[16] M. Dhimish, P. Mather, V. Holmes, Evaluating power loss and performance ratio of hot-spotted photovoltaic modules, IEEE Trans. Electron Devices 65 (12) (2018) 5419–5427.
[17] S. Ben-Yaakov, A. Cervera, A. Blumenfeld, M.M. Peretz, Resonant Switched-Capacitor Gyrator-type Converter with Local MPPT Capability for PV Cells". U.S. Patent No. 9,906,189, U.S. Patent and Trademark Office, Washington, DC, Feb. 2018.
[18] M. Dhimish, Assessing MPPT techniques on hot-spotted and partially shaded photovoltaic modules: comprehensive review based on experimental data, IEEE Trans. Electron Devices 66 (2019) 1132–1144.
[19] P. Mao, Y. Wei, H. Li, J. Wang, Junction diodes in organic solar cells, Nano Energy 41 (2017) 717–730.
[20] M. Bressan, A. Gutierrez, L.G. Gutierrez, C. Alonso, Development of a real-time hot-spot prevention using an emulator of partially shaded PV systems, Renew. Energy 127 (2018) 334–343.
[21] M. Dhimish, 70% decrease of hot-spotted photovoltaic modules output power loss using novel MPPT algorithm, IEEE Trans. Circuits Syst. II Express Br. (2019).
[22] G. Nolze, A. Winkelmann, A.P. Boyle, Pattern matching approach to pseudo-symmetry problems in electron backscatter diffraction, Ultramicroscopy 160 (2016) 146–154.
[23] X. Zhang, X. Cen, R. Ravichandran, L.A. Hughes, K. van Benthem, Simultaneous scanning electron microscope imaging of topographical and chemical contrast using in-lens, in-column, and everhart–thornley detector systems, Microsc. Microanal. 22 (3) (2016) 565–575.
[24] P. Bharadwaj, K. Karnataki, V. John, June). Formation of hotspots on healthy PV modules and their effect on output performance, in: 2018 IEEE 7th World Conference on Photovoltaic Energy Conversion (WCPEC)(A Joint Conference of 45th IEEE PVSC, 28th PVSEC & 34th EU PVSEC), IEEE, 2018, pp. 0676–0680.
[25] H.J. Solheim, H.G. Fjær, E.A. Sørheim, S.E. Foss, Measurement and simulation of hot spots in solar cells, Energy Procedia 38 (2013) 183–189.
[26] I. Geisemeyer, F. Fertig, W. Warta, S. Rein, M.C. Schubert, Fast Hot Spot Evaluation, 29th EUPVSEC Amsterdam, 2014, pp. 2429–2434.